Journal of
Nanoscience and Nanotechnology
Vol. 11, 5469–5475, 2011

Influence of Cation Nature on Stabilization of Gold Nanospecies in Mordenites

I. Tuzovskaya[1, 2], E. Lima[3, 4], P. Bosch[4], N. Bogdanchikova[2, *], A. Pestryakov[5], and J. Fraissard[6]

[1] *Catalytic Processes and Materials, University of Twente, P.O. Box 217, 7500 AE Enschede, The Netherlands*
[2] *Centro de Nanociencias y Nanotecnología, Universidad Nacional Autónoma de México, Apdo. Postal 2681, C. P. 22800, Ensenada, México*
[3] *Universidad Autónoma Metropolitana, Iztapapala, 09340 México D.F., México*
[4] *Instituto de Investigaciones en Materiales, Universidad Nacional Autónoma de México, Ciudad Universitaria, México D. F., México*
[5] *Tomsk Polytechnic University, Tomsk 634050, Russia*
[6] *P. and M. Curie University, ESPCI, laboratoire lpem, 75005, Paris, France*

Gold species deposited on NH_4^+- and H^+-mordenites were studied by X-ray diffraction, xenon adsorption, NMR of ^{27}Al and ^{129}Xe, UV-Visible spectroscopy and TPR. Mordenite ion-exchange cations exert a significant effect on size distribution and electronic state of gold species supported on the zeolites. $AuNH_4M$ contains larger nanoparticles of gold on its external surface than AuHM because protonic form of zeolite has stronger sites for stabilization of gold nanospecies. In the case of NH_4^+-mordenite, Au clusters inside zeolite channels have bigger size and fill the side-pockets completely after gold deposition due to more complete reduction of gold entities, while in H^+-mordenite only half the side-pockets are filled by gold species. H^+-mordenite favors the stabilization of both small gold clusters and cations. Even after the reduction of gold by hydrogen flow at 100 °C, some gold species are not completely reduced and have certain effective charge ($Au_n^{\delta+}$ clusters).

Keywords: Gold, Zeolites, Clusters, Nanoparticles, Catalysts.

RESEARCH ARTICLE

1. INTRODUCTION

The synthesis of small metal particles is very important since nanoparticles and clusters have different catalytic properties as compared with bulk metal. For example, gold nanoparticles smaller than about 3 nm exhibit very high catalytic activity in low-temperature CO oxidation.[1, 2] Different methods of stabilizing gold particles are used, and the properties of dispersed gold are being studied intensively.[3] Zeolites are among the most interesting supports for gold due to their ability to stabilize metal clusters inside the micropores.[4, 5]

However, investigations showed that the influence of zeolite structure and method of sample preparation on the electronic and structural properties of gold is a complex function, and that a whole series of different parameters has to be considered in order to understand the real cause of the observed effects. Our previous studies revealed that the self-assembly of clusters in mordenites depends on several factors: (1) the type of zeolite crystal structure and chemical composition (SiO_2/Al_2O_3 molar ratio); (2) the acidity of the zeolite; (3) the pretreatment conditions (first of all, reduction temperature); (4) additives of metal oxides (Fe, Ni, Cu, etc.).[5–8] The influence of the gold concentration, the time and pH of ion-exchange, and the geometry of zeolites on the state of the gold was also investigated in some studies.[3, 9, 10]

To control the electronic and structural properties of nanosized gold particles is very important for the synthesis of highly active catalysts because these parameters determine the catalytic activity of gold. One of unstudied parameters influencing gold states in zeolites is the nature and size of zeolite cation.

The aim of the present study is to investigate the influence of the nature of the exchangeable cation of zeolite on the formation of gold species in Au-mordenite. For such a test we chose two types of exchangeable cations, H^+ and

*Author to whom correspondence should be addressed.

 1533-4880/2011/11/5469/007 doi:10.1166/jnn.2011.3432

NH_4^+, for the following reasons:

• the proton is the smallest and strongly acidic cation, that is important for the stabilization of gold particles;[5]

• the ammonium ion, in contrast, is the largest and less acidic cation.

2. EXPERIMENTAL DETAILS

2.1. Au/Mordenite Preparation

NH_4^+-Mordenite (NH_4M) zeolite with a SiO_2/Al_2O_3 molar ratio of 20 was supplied by Zeolist International (USA) and used as starting material. H^+-Mordenite (HM) was prepared from NH_4^+-mordenite by careful heating at 673 K, according to the usual method.[8–10]

For the preparation of Au-mordenite samples, the zeolite was mixed in aqueous solution with the $Au(NH_3)_4(NO_3)_3$ complex. $Au(NH_3)_4(NO_3)_3$ was synthesized by the method of Skibsted et al.: $HAuCl_4 \cdot nH_2O$ (49.5 wt% of Au, Alfa Aesar) was dissolved in a supersaturated solution of NH_4NO_3 and water.[11,12] A dilute solution of NH_4OH was added dropwise to this solution to bring it to pH $\sim$ 7. Then, the suspension was stirred for 24 h. After ion exchange, the samples were filtered and washed with deionized water. The washing procedure was repeated several times to remove all Cl^- ions, detected by adding $AgNO_3$ solution to a filtrate probe. The samples were dried in air at room temperature. The Au-zeolite samples were reduced with H_2 flow (20 ml/min) at 100 °C for 2.5 h using a tube furnace. The samples are denoted AuHM and $AuNH_4M$.

Gold loadings, measured by energy dispersive spectroscopy in a Jeol 5300 scanning electron microscope equipped with a Kevex Superdry detector were 2.9 and 2.5 wt% for AuHM and $AuNH_4M$, respectively.

2.2. Methods of Characterization

2.2.1. *X-Ray Diffraction*

The samples were studied by X-ray diffraction using a Bruker D8 Advance Powder Diffractometer with a copper anode tube and K_α radiation. To determine the crystallite size distributions the corresponding diffraction peaks were measured by step scanning and analyzed by the XTL-SIZE computer program.[13,14] Sample crystallinity was estimated from the sum of the peak areas and the area of the whole diffractogram. No external standard was used.

2.2.2. *^{27}Al-MAS NMR*

The spectra were recorded using a Bruker ASX 300 spectrometer operating at a resonance frequency of 78.21 MHz. Spectra were obtained in a 4-mm probe using short single $\pi/12$ pulses and a recycle time of 0.5 s. The samples were spun at 10 kHz and the chemical shifts were referenced to a 1 M $AlCl_3$ solution.

2.2.3. *Xenon Adsorption and ^{129}Xe NMR*

Pure xenon gas was used for the ^{129}Xe NMR experiment. Xenon was added to the solid in a NMR tube at 298 K and different pressures. Before xenon loading, the samples were dehydrated by gradual heating to 300 °C in vacuum (10^{-4} Torr) for 8 h. ^{129}Xe NMR spectra were recorded between −53 and 25 °C with a Bruker DMX-500 spectrometer operating at 138.34 MHz. Several scans (500–1000) were collected with a delay time of 2 s. The chemical shift was referenced to xenon gas extrapolated to zero pressure.

2.2.4. *UV-Visible Diffuse Reflectance Spectra*

UV-Visible diffuse reflectance spectra (DRS) were recorded with a Cary 300 SCAN (Varian) spectrophotometer with a standard diffuse reflectance unit. The DRS spectra presented below were obtained by subtraction of the zeolite spectra from the corresponding Au-zeolite ones.

2.2.5. *Thermo-Programmed Reduction*

Thermo-programmed reduction with hydrogen (TPR) was carried out using an Altamira Instruments AMI-1 equipped with a trap to collect traces of water and ammonia at −20 °C ahead of the thermal conductivity detector (TCD). 0.15–0.2 g of the as-prepared sample was heated at 20 °C/min from 25 °C to 550 °C in a flowing H_2/Ar mixture (1/9). The amount of H_2 consumed for the reduction of oxide species was measured by TCD and estimated from the integrated areas of the peak profiles obtained using absolute calibration of the TCD detector.

3. RESULTS AND DISCUSSION

3.1. Modification of the Zeolite Structure

Mordenite crystallinity determined by XRD decreases as gold is incorporated (Fig. 1). The crystallinity of AuHM and $AuNH_4M$ samples pretreated at 373 K for 2.5 h was 90% and 65%, respectively, as compared with 100% crystalline HM and NH_4M. The ^{27}Al MAS NMR spectra (Fig. 2) show that loading gold into mordenite promotes the formation of some extra-lattice octahedral aluminium (peak close to 0 ppm) to the detriment of tetrahedral aluminium (peak near 53.7 ppm). Furthermore, the signal due to tetrahedral aluminium becomes broader as gold is loaded.

3.2. Distribution of Gold Particle Size

The X-ray diffraction patterns show that in AuHM and $AuNH_4M$ samples pretreated at 373 K for 2.5 h the peaks corresponding to metallic gold are clearly resolved at 38.1° and 44.5° representing the formation of large nanoparticles, located on the external surface of the zeolite (Fig. 1). $AuNH_4M$ exhibits a broad size distribution from 23 to

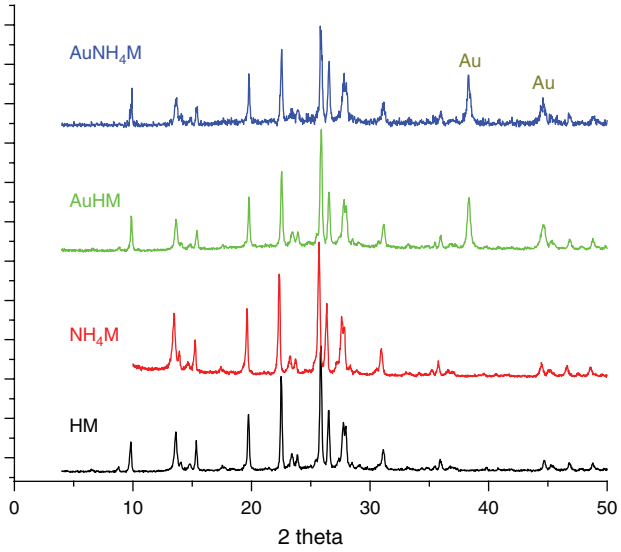

Fig. 1. X-ray pattern of pure mordenite and gold loaded mordenite samples pretreated at 100 °C for 2.5 h.

29 nm with a maximum at 28 nm (Fig. 3). AuHM contains particles of different sizes, i.e., 7–12, 19–22 and 25–30 nm. Therefore, $AuNH_4M$ contains larger nanoparticles of gold on its external surface than does AuHM. We can suppose that protonic form of zeolite has stronger sites (H^+) for stabilization of gold nanoparticles during the sample preparation.

However, it has to be emphasized that this method is valid for nanocrystalline compounds with a concentration higher than ca. 1% and for particle size larger than 2–3 nm, which can be located only on the external surface of the mordenite. For the investigation of gold clusters inside the zeolite channels we used ^{129}Xe NMR spectroscopy.

3.3. Gold Electronic State

DRS spectra of Au-zeolites as-prepared or pretreated in Ar at 300 °C for 1 h are given in Figure 4. The spectra of the

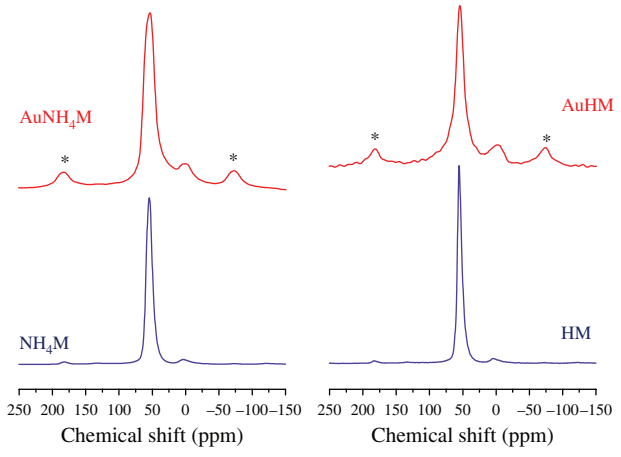

Fig. 2. ^{27}Al MAS NMR spectra of the samples. *Indicates spinning side bands.

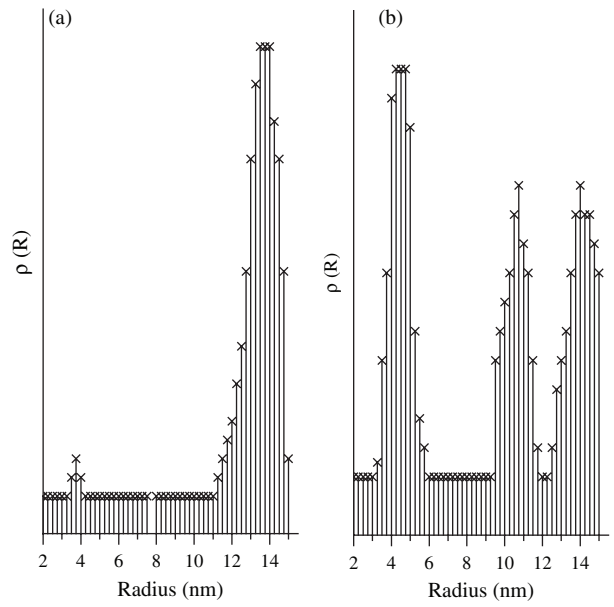

Fig. 3. Gold crystal size distribution obtained from X-ray diffraction patterns. (a) $AuNH_4M$; (b) AuHM.

as-prepared samples, which are similar in shape, have three peaks with maxima at 200, 290 and 380 nm for $AuNH_4M$ and 200, 240 and 370 nm for AuHM. The band at 200 nm can be attributed to the Au^{3+} ions; the peaks with maxima at 240 or 290 and 370 or 380 nm are assumed to characterize small charged or neutral gold clusters.[6] These bands can be related to two different types of clusters (variance in nuclearity and/or charge). Gold clusters appear just after the ion-exchange procedure, probably due to the partial reduction of gold ions inside the zeolite channels by water[6] or by the ligands of the complex.[5] A similar effect of the partial reduction of Au^{3+} by water inside the channels under ambient conditions was observed by Salama et al.[15] Optical spectra indicate a difference in size and the effective charge of gold clusters in the zeolites studied. Ion exchange proceeds inside the zeolite as well as outside, but the internal surface area is several hundred times higher than the external one. Therefore, most of the small clusters should be formed inside the zeolite channels.

In the spectra of the samples calcined at 300 °C the peak at 200 nm is decreased and a new peak at 510–530 nm appears. These peaks correspond to plasmon of gold nanoparticles.[16, 17] Obviously reduction has occurred during heat treatment but some gold ions still remain in the samples. The spectra also show that the gold clusters (bands at 230–290 nm) in zeolites are rather stable to redox treatments, probably due to their encapsulation inside the channels.

By the TPR method (Fig. 5) three peaks corresponding to the different stages of gold reduction were observed with maxima at 192, 220 (shoulder) and 312 °C for $AuNH_4M$, at 200, 230 °C and a broad shoulder around 312 °C for AuHM. The peaks at 192 and 200 °C are

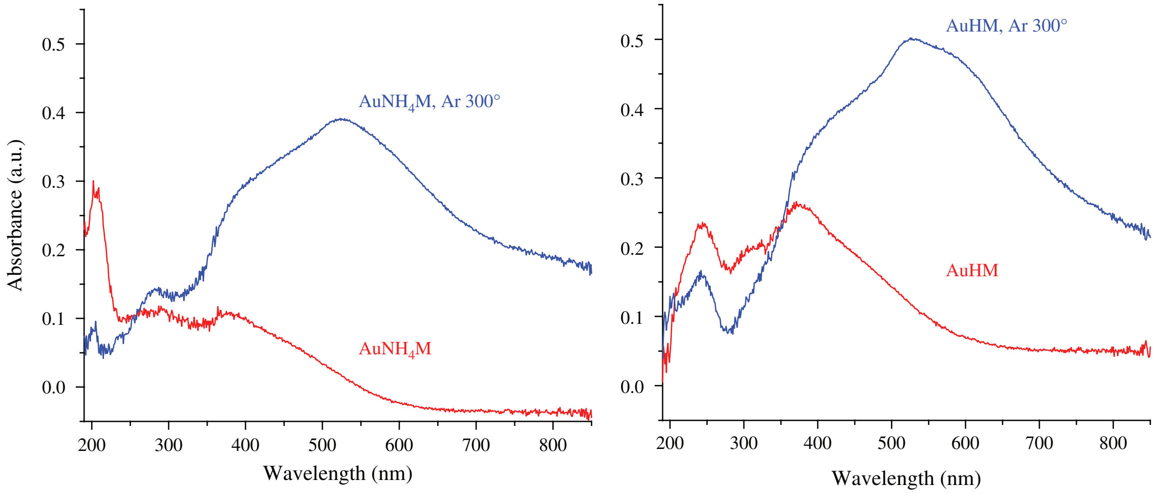

Fig. 4. UV-Visible spectra of Au-zeolites as-made and after treatment with Ar at 300 °C.

assigned to stepwise reduction of Au^{3+} to Au^{+} and Au^{+} to Au^{0}, respectively. The temperature difference of these two first peaks between samples (about 10 °C) could be due to a stronger Au^{n+}-zeolite interaction for HM zeolite than for NH_4M. The broad peak at *ca.* 312 °C could correspond to the reduction of large particles of gold oxide on the external surface of the zeolite.[18] If so, we could say that the major part of the charged gold species is located inside the zeolite channels. The relative contribution of gold particles on the external surface of AuNH$_4$M is higher than with AuHM, as already evidenced by the XRD results.

The quantity of reduced gold, calculated from the amount of hydrogen consumed during the TPR experiment, was about 50% of the overall amount of gold for both AuNH$_4$M and AuHM. According to the literature all supported ionic gold species should be reduced at 360 °C.[15] We suggest that the remainder, the 50% of the gold not observed by TPR, is already reduced before the TPR experiment. That is in agreement with the DRS data, which show the appearance of clusters (reduced species) formed during gold deposition by the ion-exchange method.

3.4. Gold Location

^{129}Xe NMR spectroscopy is a direct method for determining the location of gold in zeolites. It is well known now that xenon is a probe for zeolite pores with a diameter greater than that of xenon (0.43 nm). The amount of adsorbed xenon increases linearly with the xenon pressure (Fig. 6). For each pressure the adsorbate concentration is greater for HM than for NH$_4$M, probably because of the spatial requirements of NH_4^+. The amount of adsorbed xenon is lower for Au-mordenites than for pure mordenites. This can be due to the location of gold particles inside the channels.

Mordenite represents a two-dimensional system of crossing channels with two different elliptic cross-sections whose axes are: (a) 0.65 and 0.70 nm (main channels); (b) 0.26 and 0.57 nm (side-pockets).[19] In mordenites, the side-pockets and the main channels are available for xenon sorption.[20,21] In HM at 25 °C, the spectrum contains only one peak, due to fast exchange of xenon between the side-pockets and the main channels (Fig. 7). In order

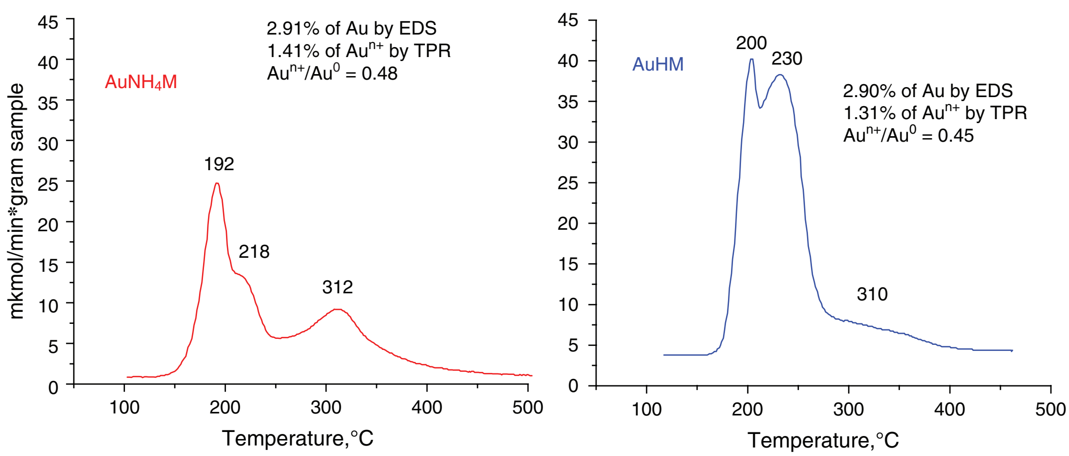

Fig. 5. TPR profiles of Au-zeolites.

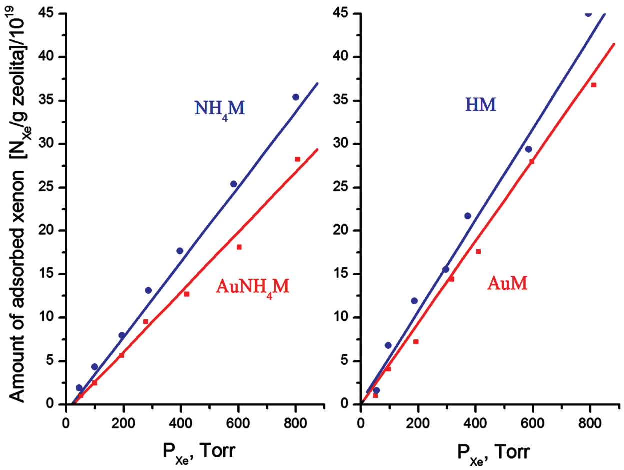

Fig. 6. Adsorption of xenon gas on mordenite samples at room temperature.

to limit this mobility, spectra must be recorded at low temperature. Figure 7 shows the evolution of the NMR spectra of xenon in HM with temperature. Initially HM was exposed at 300 Torr of xenon at room temperature. The two peaks at *ca*. 205 and 141 ppm corresponding to xenon located in side-pockets and main channels, respectively, are clearly resolved at −53 °C. In addition, the chemical shift of xenon adsorbed in the main channels slightly increases as the concentration raises with temperature decrease. The chemical shift corresponding to the side-pockets is constant because each one can adsorb only one Xe atom. In fact, we think that only a small fraction of a Xe atom enters the side-pocket, because the Xe diameter (0.43 nm) is much bigger than the small axis of the side pocket cross-section (0.26 nm).

In the spectra of AuHM the two peaks are shifted from 205 to 238 ppm and from 141 to 150 ppm for Xe in side-pockets and in main channels, respectively (Fig. 8). This result indicates that gold particles are hosted in both

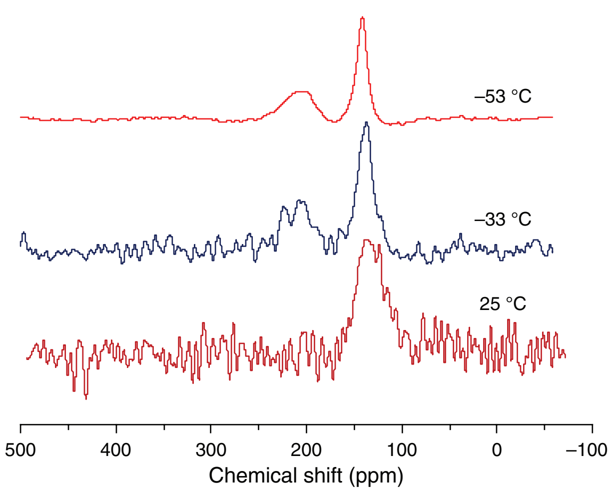

Fig. 7. Temperature dependence of the [129]Xe NMR spectrum in H-mordenite sample equilibrated at 300 Torr of xenon.

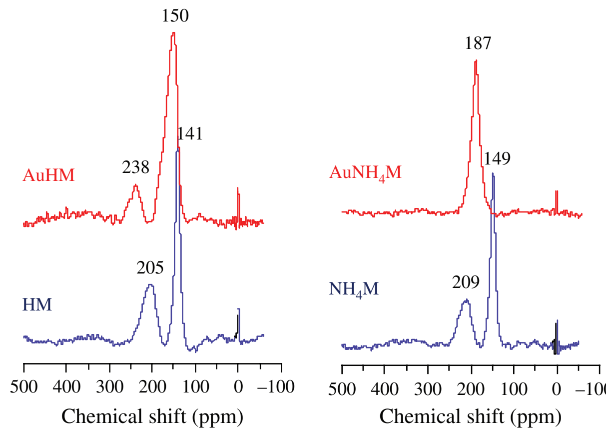

Fig. 8. ^{129}Xe NMR spectra recorded at −53 °C (P_{Xe} = 300 Torr).

sites. The gold entities inside the side-pocket must be small in order to leave some space available for xenon. Those could be cationic species of gold with radii of 0.085 and 0.137 nm for Au^{3+} and Au^{+}, respectively, as well as charged gold clusters such as $Au_n^{\delta+}$ (n = 2–8). Clusters with more than 8 atoms are not compatible with the side-pocket dimensions.

In contrast to AuHM, the side-pockets of $AuNH_4M$ are blocked to xenon sorption (Fig. 8). In $AuNH_4M$ sample the formed clusters are probably bigger than those in AuHM due to a more complete reduction of gold entities. It may be caused by reducing properties of ammonium ions. It is confirmed indirectly by TPR data (Fig. 5). TPR revealed, that total portion of ionic gold is similar in both zeolites (48 and 45 wt%). However, in contrast with AuHM in $AuNH_4M$ significant part of gold ions is located in the form of gold oxide particles on the external surface of support and portion of reduced gold inside the channels is much higher. Moreover, NH_4^+ ions partly remaining in zeolite after ion-exchange process have larger diameter as compared with H^+ and occupy more space in channels and side-pockets.

Another difference is observed between the spectra of the Au-mordenites: a narrow peak assigned to xenon in the main channels is observed in $AuNH_4M$, but the corresponding signal of AuHM is broad and asymmetric, suggesting that it consists of at least two peaks (Fig. 8). This difference suggests that the metal is more homogenously dispersed in $AuNH_4M$ than in AuHM. This broad, asymmetric peak could be due to a relatively wider distribution of either the particle sizes or the gold effective charge in various channels. Furthermore, the chemical shift of this signal is significantly higher for $AuNH_4M$ (187 ppm) than for AuHM (150 ppm), which means that the gold particles stabilized in the main channels of $AuNH_4M$ are either more charged or in higher concentration.

In Figure 9 the variations of chemical shift with the amount of Xe adsorbed in the main channel of AuHM and $AuNH_4M$ present a slightly pronounced minimum at low

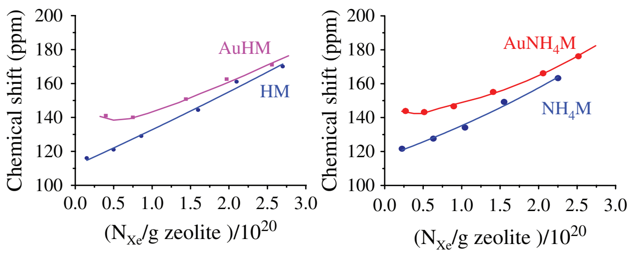

Fig. 9. Chemical shift of ^{129}Xe NMR signal (at 220 K) as a function of xenon amount adsorbed in the various samples.

Xe concentration, which indicates the interaction of Xe with charged gold species. Slightly charged gold particles were already detected by Xe-NMR and by IR in the case of AuY samples.[11] Non-pronounced minimum on the plots of Figure 9 indicates that the effective charge of gold clusters is not high as compared, for example, with extra-lattice aluminium ions which showed very pronounced minimum due to stronger interaction of high-charged ions Al^{3+} with Xe atoms.[22]

Thus, a difference in the stabilization of gold species inside the mordenite with two different types of cations was observed. The NH_4^+ cation is much larger (0.29 nm) than H^+. The size of $Au(NH_3)_4^{3+}$ is about 0.7 nm. It could be difficult for it to diffuse in the main channels whose cross-section is 0.65×0.70 nm containing NH_4^+ ions. Thus, the Au^{3+} cation has to lose at least some of its ligands to enter the channels. In the case of HM the protons do not impede diffusion of the complex. But, in this case, decomposition of the complex could also occur due to the strong interaction between the acidic H^+ sites and the NH_3 ligands. Gold–ammonia complexes are unstable in acidic media.[12]

Thus, we suggest that $Au(NH_3)_4^{3+}$ loses ligands when it enters the mordenite channels and then Au^{3+} could be reduced by the ligands. Investigation of the mechanism of these processes requires further experiments.

4. CONCLUSIONS

Comparative study of protonic (minimum cation size) and ammonium (one of the largest cation size) mordenite forms revealed that nature and size of cation do not influence the portion of gold clusters (approximately a half) formed at room temperature during ion-exchange step. However, nature of mordenite cation exerts a significant effect on the state of gold species located both on external surface of the support and inside the zeolite channels, size distribution of nanoparticles, location of clusters inside zeolite channels as well as electronic state and redox properties of gold ions. HM favors the stabilization of small gold clusters, cations and smaller nanoparticles because protonic form of zeolite has stronger sites (H^+) of gold stabilization than $AuNH_4M$ (NH_4^+), which prevent aggregation of reduced species. As a result, AuHM contains higher contribution of small nanoparticles of gold with size 8–10 nm on external surface than $AuNH_4M$; its gold clusters inside zeolite channels have smaller size and therefore only half the side-pockets are filled, while in $AuNH_4M$ gold clusters fill the side-pockets completely. This can also be caused by more complete reduction of gold cations located inside NH_4M due to reducing properties of ammonium ions in contrast with protons in HM.

Portion of ionic gold in the fresh samples is similar in both zeolites (48 and 45 wt%). However, according to TPR data in $AuNH_4M$, in contrast with AuHM, significant part of gold ions is located in the form of gold oxide particles on the external surface of the support. Even after the reduction of gold by H_2 at 100 °C, some gold species are not completely reduced and have certain effective charge ($Au_n^{\delta+}$ clusters).

Results obtained in this work are important for controlling the electronic and catalytic properties of gold species inside pores and channels during the preparation of Au/zeolite catalysts.

Acknowledgments: The authors would like to express their gratitude to E. Flores, J. A. Peralta, P. Casillas, I. Gradilla, M. Sainz, C. Gonzalez, and J. Palomares for valuable technical assistance with the experimental work. This work was supported by CONACYT grant No 79062 and 24676, PAPIT-UNAM IN100908 (Mexico) and by RFBR grant 09-03-00347-a (Russia).

References and Notes

1. M. Haruta, N. Yamada, T. Kobayashi, and S. Iijima, *J. Catal.* 115, 301 (**1989**).
2. M. Valden, X. Lai, and D. W. Goodman, *Science* 281, 1647 (**1998**).
3. G. C. Bond, C. Louis, and D. T. Thompson, Catalysis by Gold, Imperial College Press, London (**2006**).
4. D. Guillemot, M. Polisset-Thfoin, and J. Fraissard, *Catal. Lett.* 41, 143 (**1996**).
5. A. Simakov, I. Tuzovskaya, A. Pestryakov, N. Bogdanchikova, V. Gurin, M. Avalos, and M. H. Farías, *Appl. Catal. A* 331C, 121 (**2007**)
6. I. Tuzovskaya, N. Bogdanchikova, A. Simakov, V. Gurin, A. Pestryakov, M. Avalos, and M. H. Farías, *Chem. Phys.* 338, 23 (**2007**).
7. E. Smolentseva, N. Bogdanchikova, A. Simakov, A. Pestryakov, I. Tuzovskaya, M. Avalos, M. Farías, A. Díaz, and V. Gurin, *Surf. Sci.* 600, 4256 (**2006**).
8. E. Smolentseva, N. Bogdanchikova, A. Simakov, A. Pestryakov, M. Avalos, M. H. Farias, A. Tompos, and V. Gurin, *J. Nanosci. Nanotechnol.* 7, 1882 (**2007**).
9. J. Lin and B. Wan, *Appl. Catal. B: Environ.* 1257, 1 (**2002**).
10. J. Lin and B. Wan, *Appl. Catal. B: Environ.* 41, 83 (**2003**).
11. D. Guillemot, V. Y. Borokov, V. B. Kazansky, M. P. Polisset-Thfoin, and J. Fraissard, *J. Chem. Soc., Faraday Trans.* 93, 3587 (**1997**).
12. L. H. Skibsted and J. Bjerrum, *Acta Chem. Scand.* A28, 740 (**1974**).

13. A. G. Alvarez, R. D. Bonetto, D. M. Guerín, A. Plastino, and L. Rebollo-Neira, *Powder Diffr.* 2, 220 **(1987)**.
14. R. D. Bonetto, H. R. Viturro, and A. G. Alvarez, *J. Appl. Crystal.* 23, 136 **(1990)**.
15. T. M. Salama, T. Shido, R. Ohnishi, and M. Ichikawa, *J. Phys. Chem. B* 100, 3688 **(1996)**.
16. U. Kreibig and M. Vollmer, Optical Properties of Metal Clusters, Springer-Verlag, Berlin **(1996)**.
17. I. V. Tuzovskaya, A. V. Simakov, A. N. Pestryakov, N. E. Bogdanchikova, V. V. Gurin, M. H. Farías, H. J. Toznado, and M. Avalos, *Catal. Commun.* 8, 977 **(2007)**.
18. J. H. Chen, J. N. Lin, Y. M. Kang, W. Y. Yu, C. N. Kuo, and B. Z. Wa, *Appl. Catal. A: General* 291, 162 **(2005)**.
19. W. M. Meier and D. H. Olson, Atlas of Zeolite Structure Types, Butterworth-Heineman, Boston **(1992)**.
20. T. Ito, L. C. D. Menorval, E. Guerrier, and J. Fraissard, *Chem. Phys. Lett.* 3, 271 **(1984)**.
21. J. Nagano, T. Eguchi, T. Asanuma, H. Masui, H. Nakayama, N. Nakamura, and E. Derouane, *Micr. Mes. Mater.* 33, 249 **(1999)**.
22. A. Ribotta, M. Lezcano, M. Kurgansky, E. Miro, E. Lombardo, and J. Petunch, *Catal. Lett.* 49, 77 **(1997)**.

Received: 27 November 2009. Revised/Accepted: 25 January 2010.